

BLOCK ADJUSTMENT OF LINEAR PUSHBROOM IMAGERY WITH GEOMETRIC CONSTRAINTS

Chris McGlone
Digital Mapping Laboratory
School of Computer Science
Carnegie Mellon University
5000 Forbes Avenue
Pittsburgh, PA 15213-3891 USA
1-(412)-268-2524, 1-(412)-268-5576 (fax)
jcm@cs.cmu.edu
Commission II, Working Group 6

KEY WORDS: block adjustment, linear pushbroom, geometric constraints, multispectral/hyperspectral imagery

ABSTRACT

This paper describes experiments in the block adjustment of linear pushbroom sensor imagery incorporating object-space straight line constraints. Both polynomial and interpolative platform models were tested; the polynomial model generally performed better than the interpolative model without lines, but not as well as the interpolative model with straight line constraints. The greater flexibility of the interpolative model makes it better able to describe complex platform motion and to utilize the geometric strength given by the straight line constraints, at the expense of increased sensitivity to uneven point distributions or bad points.

1 MOTIVATION

Linear pushbroom imaging sensors have become widely used within the last few years as a cost-effective means to obtain aerial digital imagery. Linear arrays are less expensive to fabricate than area arrays and require no moving parts, unlike scanners or panoramic cameras.

The main drawback to the use of linear pushbroom sensors is their weak geometry; each image line is, in effect, an independent one-dimensional image. Resecting an individual line is an indeterminate problem, while using the whole image requires that a model of the platform motion as a function of time be solved. The availability of accurate navigation data such as differential GPS and high-resolution Inertial Navigation System (INS) sensors has alleviated this problem somewhat. Another approach has been to use multiple linear arrays, pointing in the nadir and off-nadir directions, to improve the geometry by obtaining a wider cone of rays from the same sensor position and also to allow stereo viewing. Examples of this configuration include the MEOSS and MOMS-02 sensors [Ohloff, 1995].

This paper describes block adjustment experiments using linear pushbroom and frame imagery. This solution differs somewhat from current practice in that only limited navigation information (nominal GPS positions) was available, due to equipment problems during data acquisition. While these experiments may not appear directly relevant to the state of the art, they are important for several reasons:

- From a practical standpoint, navigation equipment sometimes fails and reflights are not always an option. Alternative methods of positioning can be necessary.
- Navigation information may not provide sufficient absolute positioning accuracy, due to the inherent errors of the navigation sensors. As higher-resolution digital imagery becomes available, the positioning requirements will become greater. These requirements may be met by improving navigation sensors or by adding additional information to the solution; the choice is a matter of the economics of the particular system. A

related issue is the discrete nature of the positioning information, which is available only at intervals. Sensor behavior between readings must be interpolated, on the assumption that the characteristics of the platform motion do not change. Adding external information between reference points will make this interpolation more valid.

- An increasing amount of work is currently being devoted to the fusion of imagery from different sensors, taken at different times. While each set of imagery may be positioned to some level of absolute accuracy, the accumulated relative error between image sets may make fusion difficult. A simultaneous adjustment of all the imagery, with additional information in the form of tie points and geometric constraints, is necessary in such a case.
- Positioning from navigation data alone is inherently open-loop, in that there is no external verification or redundant determination of the positions. For this reason, most block solutions based on navigation information utilize a few control points to establish the datum and for verification purposes. This level of redundancy is adequate for well-calibrated photogrammetric systems; however, for experimental remote sensing systems such as the HYDICE, which are not designed as mapping systems, the system calibration may not be sufficient for reasonable positioning accuracy. Including external data can provide assurances on the quality of the results and also insights into any calibration deficiencies.

Our main topics in these experiments were evaluating the differences between polynomial and interpolative platform models and evaluating the use of geometric information, straight lines in the scene, to improve the block adjustment.

Our interest in HYDICE positioning is driven by two main goals. First, we want to generate high-resolution surface material maps, for densification of land-cover information and for realistic material rendering in visual simulation databases

[Ford *et al.*, 1998]. Our second goal is to support work in the fusion of disparate types of image information, in order to improve cartographic feature extraction [Ford and McKeown, 1992; Ford *et al.*, 1997]. While some amount of mis-registration can be corrected by local refinement during the fusion process, an inaccurate initial registration greatly increases the amount of down-stream work required and may adversely impact the final quality of the fusion results.

2 RELATED WORK

Most recent work on the orientation of linear pushbroom sensors has been focused on satellite sensors, especially SPOT [Kratky, 1989] and MOMS-02 [Ohloff, 1995]. This differs from the airborne problem in that the platform motion is smoother and is determined by the orbital parameters.

In airborne work, [Heipke *et al.*, 1996] summarize work on the airborne test data from the Monocular Electro-Optical Stereo Scanner (MEOSS), which uses three linear arrays, (forward-, nadir-, and backward-looking), to obtain stronger geometry. They use an interpolative platform model with full navigation information and a large number of automatically-generated tie points in a block adjustment of four image strips.

Most work on using geometric constraints for orientation has been done using frame imagery [Mikhail, 1993], applying projective geometry to relate image- and object-space lines. The research described in this paper is most closely related to [McGlone and Mikhail, 1981; McGlone and Mikhail, 1982; McGlone and Mikhail, 1985], which applied straight-line constraints in the block adjustment of airborne multispectral scanner data, and [Paderes *et al.*, 1984], which used lines in the rectification of SPOT imagery.

3 DATA SET

3.1 The HYDICE sensor

HYDICE (HYperspectral Digital Imagery Collection Experiment) is an experimental 210-channel hyperspectral imaging system developed by the Naval Research Laboratory. The HYDICE sensor is geometrically a linear pushbroom sensor 320 pixels wide; each pixel has an instantaneous field of view of 0.5 milliradians, giving a total field of view of approximately 9 degrees. Physically, the sensor is an area array, with each row of the array producing one band of the image by imaging the incident energy from a different portion of the spectrum. The spectral range of the HYDICE sensor extends from the visible to the short wave infrared regions (400 to 2500 nanometers), divided into 210 channels. The channel bandwidths range from 7.6 to 14.9 nanometers, depending on the channel location in the electromagnetic spectrum.

Ancillary navigation and environmental information is also recorded during the acquisition of HYDICE imagery. This includes INS and GPS position and orientation data, flight stabilization platform angles, and instrument engineering engineering measurements. More detailed descriptions of the HYDICE sensor system can be found elsewhere [Kappus *et al.*, 1996].

3.2 Data acquisition design

The Army base at Fort Hood, Texas, has been the subject of concentrated feature extraction research under the RADIUS program [Firschein and Strat, 1997] and other research programs, and a variety of image, cartographic, and ground

truth data sets are currently available. To build on this infrastructure, the Digital Mapping Laboratory planned and coordinated the acquisition of nine HYDICE flightlines over the Fort Hood motor pool and barrack areas. Each HYDICE flightline has a ground sample distance (GSD) of 2 meters, from an altitude of approximately 4,000 meters above ground level, and is 0.64 by 12.6 kilometers [Ford *et al.*, 1997].

The data was flown in October, 1995; unfortunately, equipment failures during flight and some problems in system integration resulted in most of the navigation data being unusable. Turbulent atmospheric conditions, unavoidable due to sensor scheduling constraints, also degraded the geometry of the imagery.

4 MATHEMATICAL MODEL

The mathematical model has several different parts; the sensor model, which describes the imaging geometry of the linear pushbroom sensor, the platform model, a representation of the aircraft position and orientation with respect to time, and the block adjustment incorporating the geometric (straight line) constraints. This section discusses each aspect of the mathematical model.

4.1 Linear pushbroom sensor model

A linear pushbroom sensor can be thought of as a frame sensor with only one line in the x , or flight line, direction. The collinearity equations, modified for use with linear pushbroom imagery, are [McGlone, 1996]:

$$\begin{aligned} \begin{bmatrix} U \\ V \\ W \end{bmatrix} &= M_{3,3} \begin{bmatrix} X_p - X_c \\ Y_p - Y_c \\ Z_p - Z_c \end{bmatrix} \\ 0 &= \frac{U}{W} \\ y - y_0 &= -f \frac{V}{W} \end{aligned} \quad (1)$$

where the x coordinate is 0, y is the image coordinate and y_0 is the principal point along the sensor, f is the focal length, and X_p, Y_p, Z_p are cartesian world coordinates of the point. The position parameters, X_c, Y_c, Z_c , and the angular orientation parameters ω, ϕ, κ , (which determine the orientation matrix $M_{3,3}$) are given by the platform model as functions of time, or equivalently, of line number.

Not all of the six orientation parameters can usually be recovered in a resection solution, due to the linear sensor geometry. The ϕ (pitch) angle is highly correlated with position along the flight line, while the narrow field of view and lack of terrain relief means that the ω (roll) angle is correlated with the cross-strip position. Without external information, such as angles or positions from navigation sensors, the ω and ϕ parameters must be held to 0 in the adjustment.

4.2 Platform model

The platform model describes the behavior of the orientation parameters as a function of time or line number. Two different models were studied in this work, the polynomial model and the interpolative model.

Polynomial platform model In the polynomial platform model, the value of each parameter ($X_c, Y_c, Z_c, \omega, \phi, \kappa$) at a particular line is written as a polynomial function of line

number x . The block adjustment solution determines the polynomial coefficients, instead of the parameters themselves.

To model complex platform motions over a long period of time would require high-order polynomials, which could lead to unstable solutions. Instead, the flight line is divided into sections, with each section having its own set of lower-order polynomials (in this case, cubic). Continuity constraints on the orientation parameters at the section boundaries ensure that calculated ground positions are continuous across the boundary.

Interpolative platform model The interpolative model stores the orientation parameters of reference lines at regular intervals, then calculates the parameters of intervening image lines by polynomial interpolation. In this case, two reference lines on either side of the line of interest are used, resulting in a cubic interpolation polynomial [Press *et al.*, 1989].

The interpolative model has become more widely used in recent years since navigation data is usually available to specify the parameters of the reference lines. When no navigation data is available, as is the case with this data set, the parameters of each reference line must be solved in the adjustment. If no control or tie points are within the interpolation range of a particular reference line, the parameters of that line will not be adjusted. A continuity constraint is therefore applied between reference lines, to ensure that all lines have consistent parameters.

4.3 Block adjustment procedure

The bundle block adjustment is performed using an object-oriented photogrammetry package [McGlone, 1995] which allows the utilization of images with different geometries and the rigorous incorporation of geometric constraints.

4.4 Straight line geometric constraints

Straight line constraints effectively provide a tie point in each image line, particularly important in this case where no navigation data is available and the imagery is severely deformed. The straight lines are easy to obtain interactively from the imagery, and do not require field surveying or additional navigational equipment.

The equation of a straight line is written as [Mikhail, 1993]:

$$\alpha(X - X_0) + \beta(Y - Y_0) + \gamma(Z - Z_0) = 0 \quad (2)$$

The line equation has six parameters, 4 of which are independent. The direction of the line is represented by the direction cosines α, β, γ , while the location is fixed by specifying the coordinates of a reference point on the line, X_0, Y_0, Z_0 , and constraining that point to be the point on the line closest to the origin.

Two additional constraint equations are required:

$$\begin{aligned} \alpha^2 + \beta^2 + \gamma^2 &= 1 \\ X_0 \alpha + Y_0 \beta + Z_0 \gamma &= 0 \end{aligned} \quad (3)$$

The first constraint normalizes the direction cosines, while the second constraint equation is necessary to give a unique definition of the reference point.

Saying that the projection of an image point, x_i, y_i , lies on a given line in object space is equivalent to saying that the

vector (image ray) from the perspective center, X_c, Y_c, Z_c , through the image point, with direction cosines $\alpha_i, \beta_i, \gamma_i$ is coplanar with the line vector α, β, γ through point X_0, Y_0, Z_0 . This is expressed by the scalar triple product:

$$\begin{vmatrix} X_0 - X_c & Y_0 - Y_c & Z_0 - Z_c \\ \alpha & \beta & \gamma \\ \alpha_i & \beta_i & \gamma_i \end{vmatrix} = 0 \quad (4)$$

An important consideration in the use of constraints is efficiency. This has two aspects; reducing the number of parameters involved, and formulating the equations to allow the most efficient normal equation structure. The straight line constraint is written so that point object space coordinates are not explicitly referenced in the equations, thereby reducing the number of total number of parameters in the solution. This also means that corresponding points do not have to be identified and measured on all images, thereby simplifying the measurement process.

5 EXPERIMENTAL PLAN

5.1 Source imagery

Three sets of imagery are available over Ft. Hood and will be used in the final block adjustment of the HYDICE imagery.

- The HYDICE imagery, collected in nine sidelapping flight lines with a ground sample distance (GSD) of 2 meters.
- KS-87 color frame imagery, also collected on the HYDICE flights. The KS-87 is an uncalibrated frame reconnaissance camera with a 6-inch focal length and a 5-inch format. The imagery was scanned at a 1 meter GSD.
- The RADIUS Ft. Hood imagery. These are about 40 nadir and oblique images, taken with a frame mapping camera and scanned at a GSD of 0.3 meters for the vertical images. These images have been previously block adjusted using surveyed ground control, and provide the basic geometric strength for the adjustment.

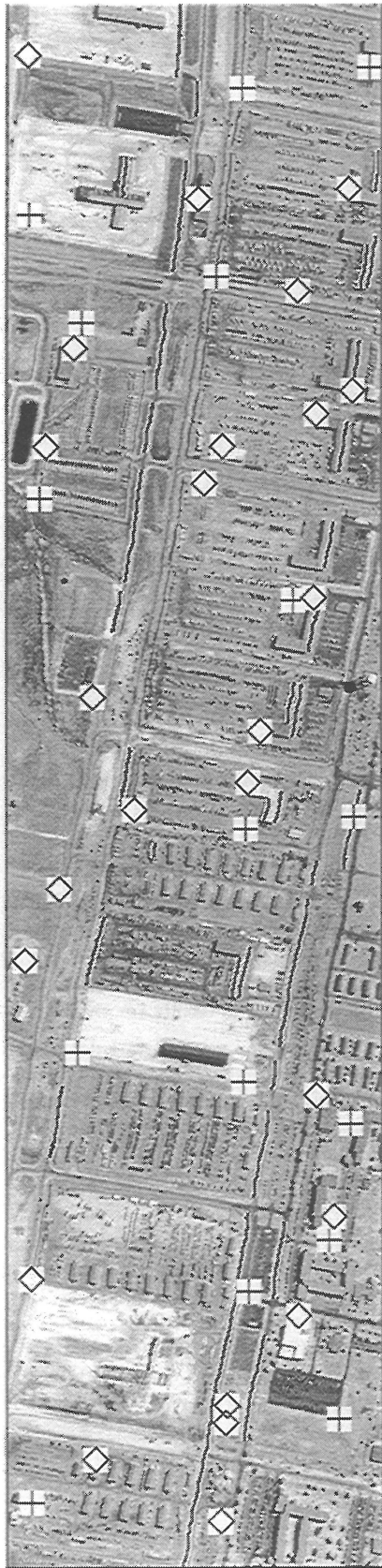
The control points for the adjustment were originally surveyed for the adjustment of the RADIUS images. Tie points are measured between all images.

5.2 Experimental data set

For the purposes of this paper, a small sub-block of the available data is being used. The sub-block includes two sidelapping 1280-line HYDICE images, four KS-87 images, and four RADIUS vertical images. Tie points between the HYDICE images and the frame images were established by manual measurement, with all tie points being measured on at least two frame images. Straight lines were also measured manually on at least two frame images. The two HYDICE images used are shown in Figure 1. Tie points for the heavy density case (described below) are shown as diamonds while check points are shown as crosses. The straight lines used in the solution are also shown.

Three levels of tie point density were established, as shown in Figure 2 and Table 1.

The same 37 check points shown in Figures 1 and 2(d) were used for each experiment. Check points which appear on both



(a) 4.3.



(b) 5.3.

Figure 1: HYDICE test images, with tie points (diamonds), check points (crosses), and constrained lines. North is to the left.

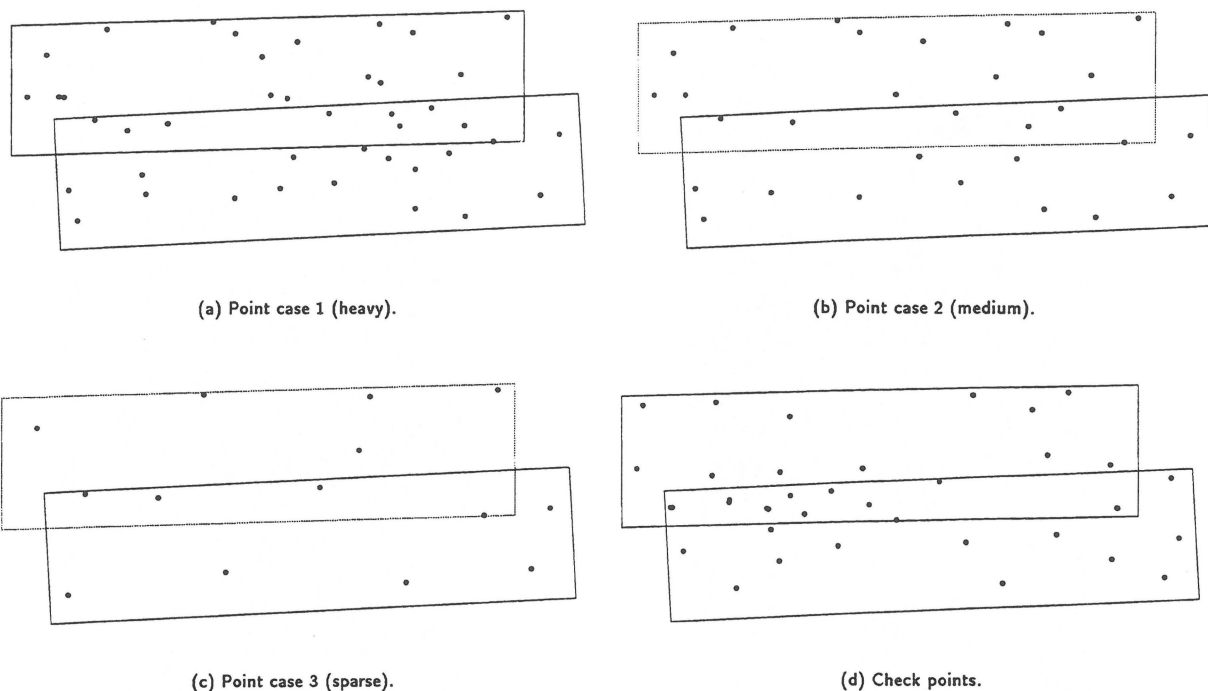


Figure 2: Point test cases, check points, and image coverages.

Case	Figure	Pts on 4_3	Pts on 5_3	Pts on both
1 (heavy)	2(a)	18	17	8
2 (medium)	2(b)	14	12	5
3 (sparse)	2(c)	6	6	3

Table 1: Point test cases.

HYDICE images are counted twice, since they are treated independently.

All measured object-space straight lines were horizontal and were constrained to be horizontal.

5.3 Evaluation procedure

Evaluation was done by comparing the calculated world X,Y coordinates of the check points against the values using the frame images. No evaluation was done on the Z coordinate, since the HYDICE sensor has a very narrow field of view (9 degrees) and elevation recovery is therefore very weak. For this reason, the Z coordinates of the check points were held fixed in the solution, and points which appeared on both HYDICE images were evaluated as two separate points. Deviations in the X, Y, and XY coordinates were calculated in a local vertical coordinate system, with X being east and Y north. In this case, X also corresponds to the along-strip direction and Y to the cross-strip direction.

In order to gain a better understanding of the characteristics of the solution, three different statistics were calculated: the median absolute deviation, the root-mean-square (RMS) deviation, and the maximum absolute deviation. Since the RMS statistic is extremely sensitive to large outliers, the me-

dian and maximum statistics are used to give a better sense of the distribution.

6 RESULTS

The results of the evaluation runs are given in Table 2 and graphically in Figure 3. The interpolative model solution for the sparse point case (3) with no lines and 32-line spacing did not converge, due to weak geometry with the reduced number of points, so no results are given.

We rely mostly on the median statistics in analyzing the results, due to the characteristics of the check point errors. The test runs show that there are often one or two very large check point deviations, not representative of the rest of the points. The RMS is greatly affected by these large values, as opposed to the median which gives a better sense of how most of the points behaved.

Polynomial vs interpolative platform models. The motion of an airborne platform can be incredibly complex, with its characteristics changing during flight. For instance, compare the differences in deformation between images 4_3 (Fig. 1(a)) and 5_3 (Fig. 1(b)), from adjacent flight lines; in particular, straight roads and buildings are much more severely deformed in 5_3 than in 4_3. Whether it is derived from navigation data, by a resection solution, or a combination of both, the platform model must meet a set of contradictory requirements. It must have enough degrees of freedom to model the actual motion with high fidelity, while too many degrees of freedom may result in an unstable solution susceptible to bad measurements. Insufficient degrees of freedom will result in aliasing, with unpredictable results between control points.

For this data set, the polynomial model generally performed better than the interpolative model without lines, but not as

Model	Pt case	Lines	Ref. line spacing	X			Y			XY		
				Med	RMS	Max	Med	RMS	Max	Med	RMS	Max
Poly	1	N	-	3.1	5.3	10.6	5.7	8.6	22.8	7.7	10.1	24.0
Poly	2	N	-	3.7	5.3	10.8	6.4	9.2	26.1	7.7	10.7	26.9
Poly	3	N	-	4.6	5.7	13.3	5.1	10.1	29.0	6.9	11.6	29.1
Poly	1	Y	-	3.1	5.2	10.6	5.7	8.6	22.8	7.7	10.1	24.0
Poly	2	Y	-	3.7	5.2	10.7	6.3	9.2	26.1	7.6	10.6	26.9
Poly	3	Y	-	4.3	5.6	13.2	5.3	10.1	29.0	6.9	11.6	29.1
Interp	1	N	32	8.0	19.9	61.8	8.1	14.3	35.4	15.5	24.5	70.3
Interp	2	N	32	11.7	21.0	58.8	9.2	15.3	42.5	17.1	25.9	67.5
Interp	3	N	32	Did not converge								
Interp	1	Y	32	3.3	4.8	12.8	4.5	8.5	30.0	5.9	9.8	30.7
Interp	2	Y	32	2.5	4.8	13.0	5.1	9.6	28.1	6.0	10.8	28.3
Interp	3	Y	32	5.2	12.3	36.7	5.9	14.0	39.4	10.2	18.7	40.5
Interp	1	N	64	8.1	11.1	27.5	9.3	13.4	32.2	13.4	17.4	37.6
Interp	2	N	64	11.1	11.9	24.8	10.5	13.9	34.4	15.5	18.3	39.2
Interp	3	N	64	12.8	20.7	56.5	15.4	23.5	51.8	24.0	31.3	58.6
Interp	1	Y	64	3.0	4.7	10.8	3.6	7.3	21.7	5.2	8.7	22.5
Interp	2	Y	64	3.2	4.7	10.8	3.4	8.2	21.7	4.8	9.4	24.1
Interp	3	Y	64	3.6	6.7	19.7	5.8	15.5	56.2	8.1	16.9	56.6

Table 2: Check point error (meters) for HYDICE images.

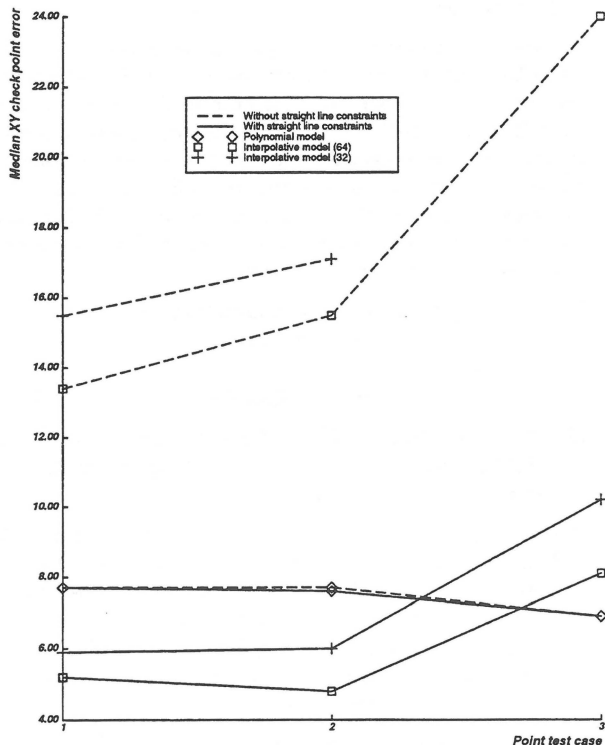


Figure 3: Median absolute XY check point error, meters.

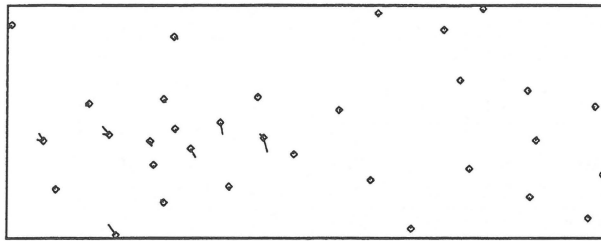
well as the interpolative model with straight line constraints. The interpolative model without straight line constraints degrades more rapidly than the polynomial model as the amount of control is decreased (going from the heavy (1) to the sparse (3) point densities). This is particularly evident in the maximum error statistic in the Y direction.

In nearly all cases, the error in the Y direction (approximately cross-strip) is worse than in the X direction (approximately along-strip). A possible explanation for this is uncompensated sensor roll, due to a combination of atmospheric turbulence and a malfunctioning stabilization platform.

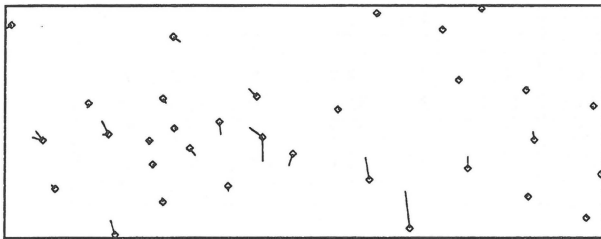
Effectiveness of straight line constraints. The inclusion of straight line constraints in the interpolative model solutions improved the results in every case. While decreasing the number of tie points still increased check point error, the results from the runs with sparse points (case 3) are still better than the results for the heavy point density (case 1) without lines. This indicates that straight line constraints can be used both to improve a solution or as an effective substitute for additional tie points. However, adding the straight line constraints to the polynomial model solution made only negligible differences. It may be that the polynomial model, with its more limited flexibility, is unable to use the additional information from the line constraints.

It is interesting to note the improvement in the X direction from the addition of the lines. The lines are selected parallel to the flight direction and would be expected to mostly improve positioning in the Y (cross-strip) direction. It is possible that, since the lines make an approximately 30-degree angle to the flight direction, they add some geometric strength in the X direction.

Reference line spacing Decreasing the reference line spacing for the interpolative model will make the model more flexible by increasing its degrees of freedom. Given enough information to determine the model, it should recreate the platform motion more accurately and give better results. In this case, however, decreasing the reference line spacing gen-



(a) Heavy point density (case 1).



(b) Sparse point density (case 3).

Figure 4: Check point errors for interpolative model with line constraints.

erally degraded the results. The additional degrees of freedom were not adequately determined by the available information, and, in fact, the solution using the sparse point density without lines did not converge.

Variation between images. As mentioned above, the characteristics of the platform motion can change drastically during a mission. The two HYDICE images used in this experiment demonstrate this; examination of Figures 1(a) and 1(b) shows that image 5_3 is much more deformed than image 4_3. Statistical evidence of this is given in Table 3 for a few selected test cases (interpolative model with line constraints). Note that the median deviations for the two images are very comparable for each case, but that the maximum check point deviations are much larger for image 5_3 than for 4_3.

Figure 4 shows the check point errors for the heavy (1) and sparse (3) point densities (interpolative model using line constraints, 64 reference line spacing). Note that check points which appear on both HYDICE images have two errors vectors, since they are treated as independent points in each image. The sparse case shows much larger check point errors for a few points; the largest for the sparse case is 56.6 meters, but 21.7 meters for the heavy case. In both cases, most points have relatively small errors, with the larger errors occurring in groups. These groupings tend to indicate areas of higher image deformation or weaknesses in the control configuration.

7 CONCLUSIONS

This work has shown the effectiveness of straight line constraints in the block adjustment of linear pushbroom imagery when used in conjunction with an interpolative platform model. The techniques demonstrated can be used in the absence of navigation data, as was the case for the HYDICE

imagery, or in conjunction with navigation data in order to improve the accuracy and reliability of the positioning solution. This work will be applied to the adjustment of our full block of HYDICE imagery, now in progress.

Despite the lack of navigation information in the current investigation, there is no theoretical or practical reason not to use these techniques in conjunction with GPS/INS data; indeed, our initial plan was to include navigation information in the block adjustment solution. Unless the navigation sensor accuracy and the system calibration are of very high order, or unless a very large number of high quality (possibly automatically generated) tie points are available, it would appear that the use of straight line constraints can make significant contributions to the accuracy of a block adjustment.

Our ongoing research will attempt to establish whether additional improvements in accuracy can be obtained or whether we are at the accuracy limits of the sensor/platform combination without the addition of further information. Possible avenues of investigation will include increasing the number of tie points by using automated measurement techniques [Heipke *et al.*, 1996] and experimentation with other types of geometric constraints, such as right angles.

8 ACKNOWLEDGEMENTS

I thank Dave McKeown and Steve Ford for their work in planning and executing the HYDICE data acquisition, Dan "Databoy" Yocum for his measurements, and the rest of my colleagues in the Digital Mapping Laboratory for their support and interaction.

The research reported in this paper was supported by the Defense Advanced Research Projects Agency (DARPA/ISO) and the U.S. Army Topographic Engineering Center under Contract DACA76-95-C-0009. The views and conclusions contained in this document are those of the authors and should not be interpreted as representing the official policies, either expressed or implied, of the U.S. Army Topographic Engineering Center, the Defense Advanced Research Projects Agency, or of the United States Government.

Digital Mapping Laboratory publications are available at <http://www.cs.cmu.edu/~MAPSLab>

REFERENCES

- [Firschein and Strat, 1997] O. Firschein and T.M. Strat. *RADIUS: Image Understanding for Imagery Intelligence*. Morgan Kaufmann, 1997.
- [Ford and McKeown, 1992] Stephen J. Ford and David M. McKeown, Jr. Information fusion of multispectral imagery for cartographic feature extraction. In *International Archives of Photogrammetry and Remote Sensing: Interpretation of Photographic and Remote Sensing Data*, volume XVII, B7, Washington, D.C., 2-14 August 1992. XVIth Congress, Commission VII.
- [Ford *et al.*, 1997] Stephen J. Ford, Dirk Kalp, J. Chris McGlone, and David M. McKeown, Jr. Preliminary results on the analysis of HYDICE data for information fusion in cartographic feature extraction. Technical Report CMU-CS-97-116, Computer Science Department, Carnegie Mellon University, Pittsburgh, Pennsylvania 15213, March 1997.
- [Ford *et al.*, 1998] Stephen J. Ford, J. Chris McGlone, Steven D. Cochran, Jeffrey A. Shufelt, Wilson A. Harvey,

Image	Pt case	Lines	Ref. line spacing	X			Y			XY		
				Med	RMS	Max	Med	RMS	Max	Med	RMS	Max
4_3	1	Y	64	4.1	4.9	9.7	3.4	3.6	5.9	6.0	6.1	9.8
5_3	1	Y	64	2.4	4.6	10.8	3.9	9.2	21.7	5.2	10.3	22.5
4_3	2	Y	64	3.9	4.8	9.6	3.5	4.6	10.9	5.6	6.6	12.5
5_3	2	Y	64	2.7	4.6	10.8	3.4	10.1	21.7	4.7	11.1	24.1
4_3	3	Y	64	3.7	8.4	19.7	4.8	7.0	14.7	8.2	10.9	24.6
5_3	3	Y	64	3.0	5.1	10.8	7.6	19.6	56.2	8.1	20.3	56.6

Table 3: Check point error (meters) on each HYDICE image, using interpolative model.

- and David M. McKeown, Jr. Analysis of HYDICE data for information fusion in cartographic feature extraction. In *Proceedings of the International Geoscience and Remote Sensing Symposium, IGARSS'98*, volume to appear, page TBD, Seattle, Washington, 6–10 July 1998.
- [Heipke et al., 1996] C. Heipke, W. Kornus, and A. Pfannenstern. The evaluation of MEOSS airborne three-line scanner imagery: Processing chain and results. *Photogrammetric Engineering and Remote Sensing*, 62(3):293–299, March 1996.
- [Kappus et al., 1996] Mary Kappus, William Aldrich, Ronald G. Resmini, and Peter Mitchell. The flexible HYDICE sensor's first year of operation. In *Proceedings of the Eleventh Thematic Conference and Workshops on Applied Geologic Remote Sensing*, volume 1, pages 433–441, February 1996.
- [Kratky, 1989] V. Kratky. Rigorous photogrammetric processing of SPOT images at CCM Canada. *Photogrammetria, Journal of the International Society for Photogrammetry and Remote Sensing*, 44:53–71, 1989.
- [McGlone and Mikhail, 1981] J. C. McGlone and E. M. Mikhail. Photogrammetric Analysis of Aircraft Multispectral Scanner Data. Technical Report CE-PH-81-3, Purdue University, School of Civil Engineering, October 1981.
- [McGlone and Mikhail, 1982] Chris McGlone and Edward M. Mikhail. Geometric constraints in multispectral scanner data. In *Proceedings of the 48th Annual Meeting, American Society of Photogrammetry*, pages 563–572. American Society of Photogrammetry, March 1982.
- [McGlone and Mikhail, 1985] J. C. McGlone and E. M. Mikhail. Evaluation of Aircraft MSS Analytical Block Adjustment. *Photogrammetric Engineering and Remote Sensing*, 51(2):217–225, February 1985.
- [McGlone, 1995] Chris McGlone. Bundle adjustment with object space constraints for site modeling. In *Proceedings of the SPIE: Integrating Photogrammetric Techniques with Scene Analysis and Machine Vision*, volume 2486, pages 25–36, April 1995.
- [McGlone, 1996] Chris McGlone. Sensor modeling in image registration. In *Digital Photogrammetry: An Addendum to the Manual of Photogrammetry*, pages 115–123. American Society for Photogrammetry and Remote Sensing, 1996.
- [Mikhail, 1993] Edward M. Mikhail. Linear features for photogrammetric restitution and object completion. In *Proceedings of the SPIE: Integrating Photogrammetric Techniques with Scene Analysis and Machine Vision*, volume 1944, pages 16–30, September 1993.
- [Ohloff, 1995] Timm Ohloff. Block triangulation using three-line images. In Fritsch, D and Hobbie, D, editors, *Photogrammetric Week 1995*, pages 197–206. Wichmann, September 1995.
- [Paderes et al., 1984] Fidel C. Paderes, Edward M. Mikhail, and Wolfgang Förstner. Rectification of single and multiple frames of satellite scanner imagery using points and edges as control. In *NASA Symposium on Mathematical Pattern Recognition and Image Analysis*, 1984.
- [Press et al., 1989] W. H. Press, B. P. Flannery, S. A. Teukolsky, and W. T. Vetterling. *Numerical Recipes In C*. Cambridge University Press, Cambridge, 1989.